LANGMUIR

pubs.acs.org/Langmuir Article

Advanced Characterization of Plastron on Cassie–Baxter Superhydrophobic Surfaces by Drop Adhesion Force

Iana Fomicheva, Petr Druzhinin, Mariia Pavlovska, Karen Ferner, Daniel Frese, George Sarau, Anca Mazare, Wolfgang H. Goldmann, Ben Fabry, Silke H. Christiansen, and Alexander B. Tesler*

Cite This: *Langmuir* 2026, 42, 8280–8289 Read Online

ACCESS | Metrics & More | Article Recommendations | SI Supporting Information

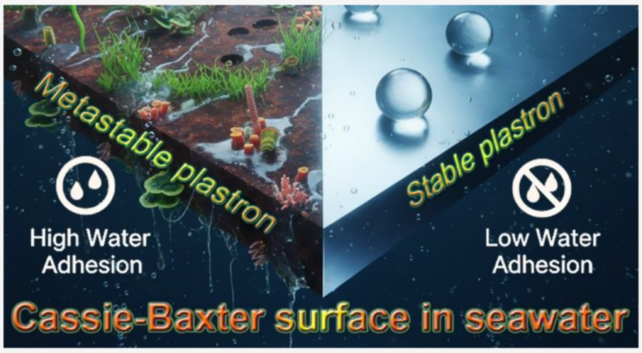

ABSTRACT: Cassie–Baxter superhydrophobic surfaces repel aqueous media by trapping a thin air layer known as plastron. However, current methods to estimate plastron characteristics on such surfaces, either directly through digital still imaging/confocal microscopy or indirectly through contact angle goniometry, are technically challenging and often imprecise. Previously, we demonstrated that the solid–liquid area fraction, which quantifies the fraction of the solid surface that is in direct contact with the surrounding liquid, can be accurately measured by reflectance optical microscopy, provided that the material surface has approximately uniform local reflectivity. To eliminate the complexity associated with optical reflectance measurements, we recently demonstrated that the drop adhesion force correlates linearly with the solid–liquid area fraction. In this study, we advance the drop adhesion force measurements obtained at different environments, compression distances, and during pressurization-hold experiments to reveal whether the plastron sustains external pressure or undergoes gradual collapse. Here, we demonstrate that measuring drop adhesion force is a robust, rapid, and technically simple method for assessing plastron properties under a wide range of environmental and surface conditions. The proposed method provides information on plastron stability within minutes and thus could aid in the design of ultrarepellent surfaces with long-term stability in demanding applications.

INTRODUCTION

Inspired by nature, researchers have been designing nonwettable surfaces, such as superhydrophobic surfaces (SHSs) that repel water, thereby enabling self-cleaning, inhibiting biofouling and corrosion, delaying icing, and enhancing water collection.[1] However, current achievements in this field fall short of meeting industrial requirements.[2] Generally, the wetting of solid surfaces is characterized by two metastable, macroscopically measured contact angles (CA), called advancing and receding contact angles. The difference between these angles, termed contact angle hysteresis (CAH), indicates droplet dynamics.[3] In practice, the apparent contact angles and the contact angle hysteresis are measured by contact angle goniometry.[4] However, the interpretation of goniometric measurements for nonwettable surfaces faces substantial challenges due to difficulties in accurately measuring extremely high contact angles and ultralow contact angle hysteresis, issues with fitting nonspherical drop shapes,[5] the unreliability in the determination of the baseline location,[6] and limitations in assessing plastron characteristics. For example, Prado et al. recently reported a 7 orders of magnitude variation in corrosion resistance of superhydrophobic aluminum substrates despite similar goniometric values.[7]

Not all superhydrophobic surfaces are resistant to wetting-related phenomena, such as biofouling, corrosion, and icing, but only those that can form continuous and stable plastron. Currently, there is no standard method for characterizing plastron, as existing microscopic[8,9] and macroscopic[10,11] measurement techniques lack lateral sensitivity and/or are technically demanding. Optical reflectance microscopy is a direct tool for measuring plastron on a macroscopic scale with microscopic resolution,[12,13] but the technique depends on the optical properties of the material surface.

In recent years, research on surface wettability has shifted toward the quantification of dynamic adhesion forces as a higher precision alternative to traditional CA goniometry.[14−18] This is because CA measurements represent an averaged combination of the solid surface energy, sample geometry, size, and characteristics of roughness and chemical heterogeneity of

Received: November 20, 2025
Revised: March 9, 2026
Accepted: March 16, 2026
Published: March 20, 2026

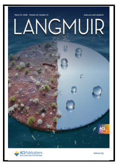

https://doi.org/10.1021/acs.langmuir.5c06133
Langmuir 2026, 42, 8280–8289

low-energy coating.[19] A range of methodologies has been demonstrated to characterize these interfacial interactions, which can be fundamentally categorized into two types: vertical adhesion (pull-off) force and lateral adhesion (friction) force.[20] Although force-based methods have provided deeper insight into the pinning mechanisms of droplets on superhydrophobic substrates,[19−26] the quantitative correlation between adhesion forces and plastron dynamics has largely been overlooked. Consequently, the relationship between the solid−liquid area fraction and the resulting adhesion forces has not been systematically determined. This leaves a fundamental aspect of the stability of the Cassie−Baxter state unresolved.

Recently, we demonstrated a simple, rapid, but indirect approach to assess the solid−liquid area fraction (SLAF) of plastron developed on superhydrophobic surfaces by measuring the drop adhesion forces (DAFs).[27] Our findings demonstrated a linear relationship between drop adhesion forces and the solid−liquid area fraction. This study further extends the drop adhesion force analysis to also assess plastron uniformity, pressure, and long-term stability in ideal and real environments. Because of its simplicity, robustness, and predictive value, the method can help to identify the most promising ultraslippery candidates for further evaluation in wetting-repellent real-world applications.

■ EXPERIMENTAL SECTION

Materials

Titanium alloy (Ti6Al4V) plates were procured from SELFAN Fine + Metal GmbH (Germany) and cut to 40 × 50 × 0.8 mm dimensions. Aluminum 1000-grade sheets of 1 mm thickness (99.5%, Al) were purchased from Advent Research Materials, UK. Hydrochloric and oxalic acids were purchased from Sigma-Aldrich, Germany, and used as received. The following products were purchased from Carl Roth (Germany): hydrogen peroxide, sodium hydroxide, acetone, and ethanol. The phosphate ester of the mixed length of fluorinated alkyl chain surfactant ($(CF_3\text{-}(CF_2)_{5-9}\text{-}(CH_2)_2\text{−}O)_2\text{-}POOH$, hereafter abbreviated as FS) was purchased from Chemguard, USA. Microfiltered natural seawater was acquired from Meerwasseraquaristik-Bartelt, Germany. Unless specified otherwise, all experiments were carried out using deionized (DI) water (18.2 MΩ · cm, ELGA, Purelab Ultra, UK).

Preparation of Aluminum Substrates

Aluminum (Al) sheets were cut into 20 × 20 × 1 mm samples for use as substrates. The substrates were first ground with SiC grinding paper up to 1200 grit. Then, the ground Al substrates were ultrasonically degreased in acetone and ethanol for 10 min each, followed by drying under a stream of N_2. The ground Al samples were pretreated in an aqueous solution of 1 M NaOH for 1 min, followed by a desmutting treatment in an aqueous solution of 1 M HNO_3 for 1 min at room temperature with stirring,[28] rinsed with DI water, and dried under a stream of N_2. These samples are termed "bare Al" (B−Al). The B−Al samples were etched stepwise in a 3 M hydrochloric acid aqueous solution, first at 40 °C for 2 min, followed by a second etching step at 80 °C for 1 min under stirring, rinsed with DI water, and then dried under a stream of N_2. The B−Al samples after the two-step etching process are termed "etched Al" (E-Al). The E-Al samples were further electrochemically anodized in an aqueous solution of 0.3 M oxalic acid at 1 °C for 30 s under an applied voltage of 60 V to form a mesoporous Al oxide layer. A two-electrode cell was used with Pt foil as the counter electrode. The distance between the counter electrode and the working electrode was about 10 mm. After anodization, the substrates were rinsed with DI water and dried under a stream of N_2. The anodized E-Al samples are termed EA-Al thereafter.

Preparation of Ti Alloy Substrates

Before anodization, the Ti alloy substrates were thoroughly cleaned using ultrasonication in acetone and ethanol for 10 min to ensure the removal of any contaminants. The clean Ti alloy samples were then electrochemically anodized. The electrochemical cell consists of a stainless steel (AISI 316) counter electrode of comparable size to a Ti alloy sheet. The Ti alloy sheet served as a working electrode, and a 1.5 M NaOH aqueous solution was used as the electrolyte. In total, 1 vol % of H_2O_2 was added to the NaOH electrolyte just before anodization. The counter and working electrodes were placed 20 mm apart. Anodization was carried out at an applied potential of 15 V for 30 min. The anodized samples were then removed from the electrolyte, rinsed with DI water, and dried under a stream of compressed air.

Low-Surface-Energy Coating

The FS surfactant, which has a surface tension of $\gamma = 15.3 \pm 0.3$ mN m^{-1} (10 g), was dissolved in 1 L of 95:5 vol % ethanol:H_2O solution using ultrasonication. The solution was stored in a closed container under ambient conditions. It is important to note that the FS solution can be reused multiple times for at least 6 years without wasting it.[7,12,13,29,30] The rough Al and Ti samples were immersed in the surface modifier solution, and a plastic cover was used to seal the surfactant container to prevent ethanol evaporation. The container with the high surface roughness samples was placed in a preheated muffle furnace set at +60 °C for 30 min. The low-surface-energy metallic substrates were then removed from the surface modifier solution, rinsed with ethanol, and dried under a stream of compressed air.

Physicochemical Characterization

We examined the surface morphology of the prepared samples using field-emission scanning electron microscopy (FE-SEM, Zeiss Crossbeam 550), equipped with energy-dispersive X-ray spectroscopy (EDX, Oxford Instruments, UK). The chemical composition of the samples was evaluated by using X-ray photoelectron spectroscopy (XPS, PHI 5600, USA). The samples were mounted on the sample holder and introduced into the ultrahigh vacuum chamber. Survey and high-resolution scans were performed to obtain detailed spectra of the core-level electrons for Al samples for C 1s, O 1s, Al 2p, F 1s, and P 2p and for the Ti alloy samples, encompassing Ti 2p and V 2p. The XPS spectra were calibrated with the C 1s peak at ≈285.2 eV for Al samples[31] and Ti 2p at 459.0 eV for Ti alloy samples. The XPS peak fitting was performed with Multipak software (version 9.8.0.19). The roughness was measured using a DCM3D confocal microscope (Leica Inc., Germany) equipped with a white LED, which combines confocal and interferometry technologies. Measurements were taken with a 20× objective. The 201 slices were measured with a step size of 0.2 μm. Topography images were then characterized using Gwyddion 2.65 software to calculate the mean area roughness (S_a) and dimensionless Wenzel roughness parameter (r_W).

Contact Angle Measurements

Water contact angles were measured using a contact angle goniometer (KRÜSS DSA25, Germany). A 5 μL drop was deposited on the surface, and the water contact angle was obtained by using the Laplace−Young fit for sessile drops. To calculate the contact angles (CAs) during infusion and withdrawal of the drop volume, which describes the dynamic wetting characteristics of a water drop on Cassie−Baxter surfaces, a 20 μL water drop volume was first dispersed on the surface. Then, the drop volume was infused to the final volume between 35 to 50 μL (depends on the sample) and thus withdrawn at a rate of 0.1 μL s^{-1} under video recording. However, it should be noted that goniometric measurements have substantial limitations when it comes to ultraslippery surfaces. First, in the context of static contact angle measurements, the extreme mobility and negligible pinning site density of these surfaces rendered standard droplet deposition ineffective.[32] The absence of a stable solid−liquid contact line caused the droplets to spontaneously depart from the surface. Second, the fitting of CAs was performed by the Ellipse method, using KRÜSS ADVANCE analysis software. It is noteworthy that the

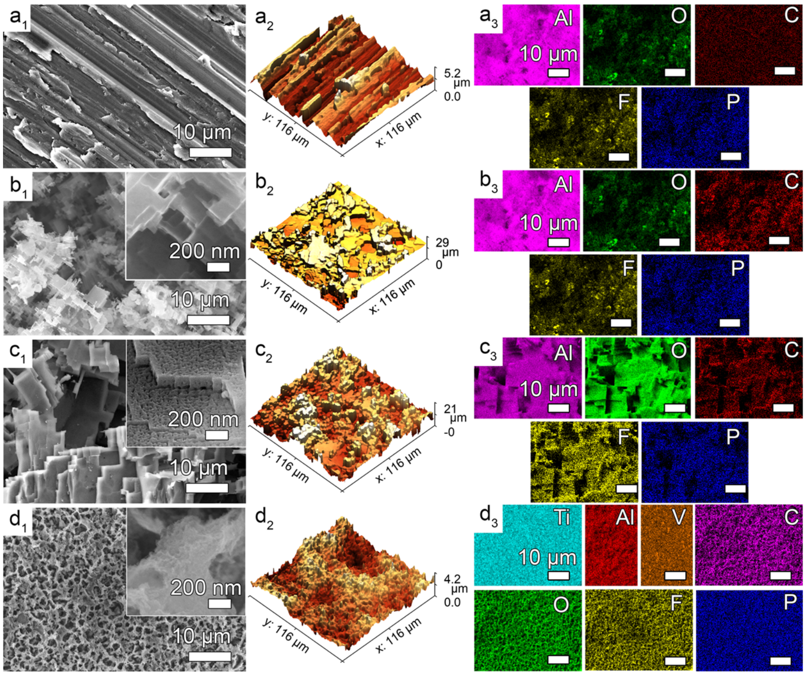

Figure 1. (a_1−d_1) Scanning electron microscopy (SEM), (a_2−d_2) 3D reconstruction of confocal microscopy, and (a_3−d_3) energy-dispersive X-ray spectroscopy (EDS) images of (a) ground Al (B−Al/FS), (b) etched Al (E-Al/FS), (c) etched/anodized Al (EA-Al/FS), and (d) anodized Ti alloy (A-Ti/FS) modified with the fluorinated surfactant self-assembly monolayer. The scale bar is equal for all of the EDS images.

calculated values obtained by the Ellipse fitting algorithm for CAs are considerably lower than those calculated by the Laplace−Young fit (Figure S1). Therefore, it is important to focus on the difference between these CAs rather than on the calculated values themselves. Third, although the limitations of the needle-in method are evident, the extreme mobility and lack of pinning sites on ultraslippery surfaces render tilting and stepwise drop build-up impractical. Therefore, the infusion/retraction drop volume is the only viable method for capturing goniometric data. All values given in the text are averaged from at least three independent measurements.

Solid−Liquid Area Fraction Measurements

A 10 cm diameter polystyrene Petri dish was filled with DI water to a height of ∼1 cm. The low-energy samples were then immersed underwater and forced to sink to the bottom. The solid−liquid area fraction was obtained using a Zeiss Axio Imager M2m light microscope with a 5x objective in bright-field reflectance mode. The solid−liquid area fraction was analyzed using MIPAR image analysis software (Version 4.5.0) with the obtained optical reflectance microscopy images. To determine the boundaries of the solid−liquid area fraction and its subsequent segmentation, Adjust Contrast and Smart Cluster Segmentation scripts were applied. The Adjust Contrast tool enhances image brightness and contrast by setting new white and black grayscale levels and then scaling the other levels accordingly. However, the E-Al/FS surface exhibits nonuniform coloration characterized by light areas with metallic luster and darker areas devoid of such shine. This results in challenges during the identification of the liquid fraction from the heterogeneous solid fraction, which comprises multiple colors. To solve this issue, smart cluster segmentation was utilized. Smart cluster segmentation assigns each pixel to one of the specified classes using k-means clustering.[33−36] The result is a grayscale image, where each class is colored according to the specified statistics of the underlying pixels. To fill each cluster, the darkest class is set to black, the brightest class is set to white, and the scale between classes is accordingly. Each cluster is filled with the mean values of the underlying pixels. In this case, three classes were selected to distinguish the liquid phase class from the two solid phase classes. For more details, we refer the reader to Section S2 in the Supporting Information. A minimum of three independent measurements were performed for each surface treatment to ensure statistical analysis.

Drop Adhesion Force Measurements

The drop adhesion forces were measured using a Tensiio force tensiometer equipped with a camera system and integrated with ADVANCE software (KRÜSS GmbH, Hamburg, Germany). A drop of deionized (DI) water was manually deposited onto the probe tip, and its mass was determined by reading the force sensor after deposition. The drop mass was adjusted to 5 μL, and the estimated standard deviation was ±3%. Given a water density of 0.997 g/cm^3 at 20 °C, the estimated standard deviation for the drop volume was 3%. The probe was brought into contact with the surface and stabilized for 0.25 s. Next, the drop was compressed by 0.4 mm at a rate of 0.01 mm s^{-1}. After achieving maximum compression, the probe was held in place for one second. Then, it was withdrawn at the same rate until the drop was fully detached from the surface or until the drop ruptured in cases of high adhesion. CAs were fitted by using the Tangential method in KRÜSS ADVANCE software. To ascertain the plastron stability, the drop of DI water was held at maximal pressure for 5 min prior to withdrawal. Here, the pressing distance was set to 0.6 mm to increase the drop footprint on the surface, thereby compensating for the drop's partial evaporation. To obtain pressure stability of plastron, the maximal compressing distance was changed between 0.2 and 0.4 mm. To determine plastron stability in a variety of environments, filtered natural seawater was utilized instead of DI water.

Note that the horizontal shift of the force−time curves between repeated measurements is due to the sample stage being raised just below the drop on the probe tip. The distance between the drop apex and the solid sample was visually controlled. Data recording begins during the instrument's automatic surface detection; however, these data are not automatically corrected to the actual contact point of 0 mm. Consequently, the distance between the drop apex and the sample surface changes by a few millimeters, causing a horizontal shift between runs.

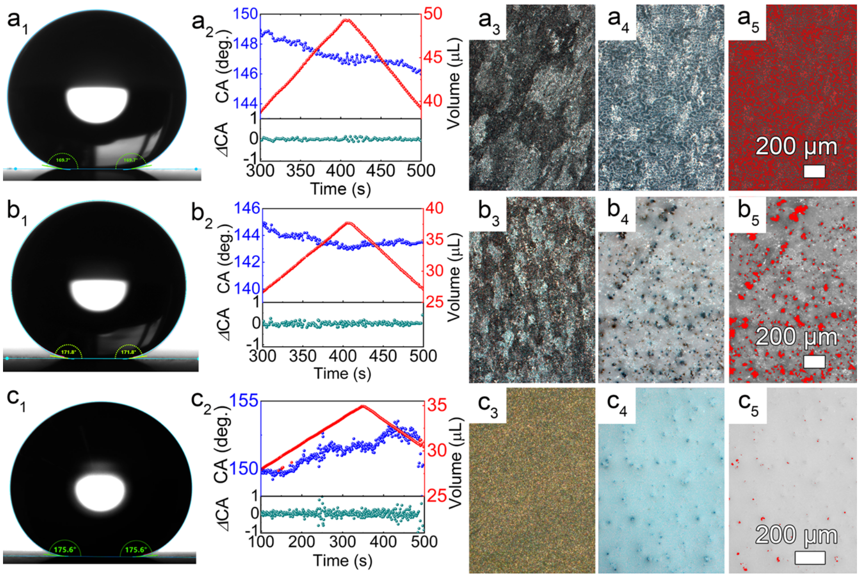

Figure 2. (a_1–c_1) Typical water CA and (a_2–c_2) slipperiness of the water drop is observed during the infusion and subsequent withdrawal of the drop volume. The measured CAs for E-Al/FS (a_1), EA-Al/FS (b_1), and A-Ti/FS (c_1) samples are 169.7°, 171.8°, and 175.6°, respectively. The CA values in (a_1–c_1) were calculated by using the Laplace–Young fitting algorithm. An error of at least ±5° should be added to these values, corresponding to the uncertainty associated with the baseline identification.[6] The CA values calculated in (a_2–c_2, blue dots) were obtained using the Ellipse fitting algorithm due to the drop's asymmetric shape and the needle inserted to increase or decrease the drop volume (red dots). Optical reflectance microscopy images (a_3–c_3) in air and (a_4–c_4) in water of (a) E-Al/FS, (b) EA-Al/FS, and (c) A-Ti/FS samples. The masked area in (a_5–c_5) is the solid–liquid area fraction calculated on the samples shown in (a_4–c_4).

■ RESULTS AND DISCUSSION

Physicochemical Characterization of the Formed Superhydrophobic Surfaces

We have developed several ultraslippery Cassie–Baxter superhydrophobic surfaces (SHSs) with comparable goniometric values, such as an apparent contact angle (CA) and contact angle hysteresis (CAH), but with substantially different plastron. Figure 1 summarizes the chemical and morphological characteristics of the developed SHS made of aluminum (Al) and titanium (Ti) alloy. In both cases, the surfaces were created by using chemical etching and/or electrochemical anodization. Figure 1a_{1-3} shows scanning electron microscopy (SEM) images, a 3D reconstruction of laser scanning microscopy images, and energy-dispersive X-ray (EDS) chemical maps of coarsely ground Al surfaces (i.e., hereafter referred to as "bare Al", B–Al) that were used for further surface treatments. The dimensionless Wenzel roughness parameter (r_W) and arithmetic mean height (S_a) of the B–Al samples were calculated by using laser scanning microscopy images and found to be 1.1 and 0.7 ± 0.1 μm, respectively (Figure 1a_2). The B–Al surfaces were then modified with a fluorinated phosphate ester surfactant (FS) to reduce their surface energy. These modified surfaces are referred to as B–Al/FS. EDS was used to characterize the surface composition of the FS-modified samples, and the results are summarized in Figures 1a_3 and S3; Table S1. As expected, the B–Al/FS samples consist of a thin native oxide layer,[30] while the FS reacts with the hydroxyl-terminated native Al oxide to form a self-assembled monolayer on the surface (Figure 1a_3). As shown in Figure 1a_3, the FS coating is patchy and not uniform. This is due to the low number of hydroxyl groups that react with the phosphate ester headgroup of the FS, as confirmed by high-resolution X-ray photoelectron spectroscopy (XPS). The O 1s peak shows lower overall intensities, while peak fitting reveals the binding energies of the native oxide at ≈530.5 eV, the P=O groups at ≈532.1 eV (can overlap with C=O and −OH groups), C–O–P groups at ≈533.0 eV, and adsorbed H_2O at 534.2 eV (Figure S4 and Table S2), which are consistent with literature.[37−39]

Goniometric and optical reflectance microscopy measurements were performed to evaluate the wetting properties and performance of the B–Al/FS surfaces. As expected, substantial plastron formation was not observed in these samples, while goniometric measurements revealed CA values of 139.5° ± 5.5° (Figure S5). Therefore, these surfaces are only hydrophobic due to their relatively low roughness and insufficient oxide content (native oxide only). This results in low surface coverage by the FS (Table S1). Thus, we applied several steps to create (*i*) hierarchical micro- and submicrometer Al surface roughness, followed by (*ii*) the formation of mesoporous anodic Al oxide layers to create superhydrophobic surfaces. Here, the B–Al samples were first chemically etched stepwise in hydrochloric acid followed by electrochemical anodization in oxalic acid. This process was previously described by us, but used here with small modifications (see the Experimental Section).[7] A two-step process is required to form micro- and submicrometer structures (Figure 1b_{1-2}). Electrochemical anodization results in the formation of a uniform mesoporous anodic Al oxide layer, introducing nano porosity and thus creating a hierarchical surface morphology (Figure 1c_{1-2}).[40] The as-etched and etched/anodized Al samples are termed E-Al and EA-Al, respectively. Morphological parameters were calculated from laser scanning microscopy images, which demonstrate Wenzel roughness parameters of 2.1 and 2.2 and arithmetic mean values of 5.4 ± 0.5 and 3.1 ± 0.1 μm for E-Al and EA-Al, respectively. It is important to note that the dimensionless (Wenzel) roughness parameter is a key value because it is used in thermodynamic frameworks to determine the stability of the developed plastron.[41−43] The arithmetic

https://doi.org/10.1021/acs.langmuir.5c06133
Langmuir 2026, 42, 8280−8289

mean value is also important, because it ensures the formation of continuous plastron. Therefore, it is important to present these parameters for any developed SHS.

The E-Al and EA-Al samples were FS-treated to reduce the surface energy. These samples are termed hereafter E-Al/FS and EA-Al/FS, respectively. EDS analysis revealed a subtle increase in oxygen content in E-Al/FS from 3.1 to 7.3 atomic percent (atom %), while after anodization, the oxygen content in EA-Al/FS increased sharply to 49 atom % (Figure S3a and Table S1). Note that the oxygen content of Al oxide in these samples overlaps with the phosphate ester headgroup of the FS. EDS analysis reveals nonuniform, patchy FS coverage of the E-Al/FS surface, comparable to that on B−Al/FS. This occurs because the etching process breaks down the protective oxide layer, while chloride ions stabilize Al complexes and prevent repassivation.[44] Thus, the etching process does not yield a sufficient amount of Al oxide, while the increase in the oxygen content is attributable to the rise in the overall surface area. In contrast, the EA-Al/FS samples demonstrate a uniform FS distribution due to an anodically formed mesoporous Al oxide layer (Figure 1b_3−c_3). The XPS analysis confirms the FS surface coverage in both samples. A slight increase in the FS coating is observed in the EA-Al/FS samples (see spectra for C 1s, F 1s, O 1s, and atomic percentages in Figure S6 and Table S3).

The wetting properties of E-Al/FS and EA-Al/FS were examined by goniometric and optical reflectance microscopy imaging techniques. The E-Al/FS and EA-Al/FS have comparable apparent CAs of 168.2° ± 7.2° and 170.7° ± 7.0°, respectively (Figure 2a_1−b_1). They also demonstrate slipperiness throughout the infusing and withdrawal drop volume steps (Figure 2a_2−b_2). Note that 5° was added to the standard deviation of the CA measurements, as suggested by Liu et al.,[6] indicating an inaccuracy in identifying the triple-phase baseline in superhydrophobic surfaces. Additionally, the CA values obtained through the infusion and withdrawal of the drop volume were fitted using the Ellipse fit rather than the Laplace−Young (L−Y) fit due to the asymmetric shape of the drop and the inserted needle. Since the Ellipse-fitted CAs do not accurately represent the values obtained by the L-Y fit (Figure S1), the first derivative (ΔCA) was calculated (Figure 2a_2−b_2, bottom plots). The latter denotes the relative change in the fitted CAs between subsequent frames through the infusing and withdrawing drop volumes, distinguishing between pinned or sliding drops. As shown in Figure 2a_1−b_1,a_2−b_2, both Al superhydrophobic surfaces exhibit comparable apparent CAs and drop slipperiness.

Although the goniometric measurements are substantially similar, the plastron shape and coverage differ considerably (Figure 2a_3−b_3,a_4−b_4). In the case of E-Al/FS, the plastron has an irregular, worm-like shape with a solid−liquid area fraction as high as 57 ± 3% (Figures 2a_3−a_5 and S7). The presence of nonuniform background coloration in the E-Al/FS samples complicates plastron identification. Conversely, the EA-Al/FS samples show a continuous plastron shape (bright gray color area) with randomly distributed pinning points, i.e., dark round spots (Figure 2b_4). The solid−liquid area fraction in the EA-Al/FS samples was measured using optical reflectance microscopy imaging, yielding a result of 9 ± 2%, i.e., a 6-fold decrease compared to the E-Al/FS samples. In this case, the nonuniform background does not overlap with plastron measurements because the latter is continuous, and the microscope is focused on the water−air interface rather than the air−solid interface (Figures 2b_5 and S8).

Finally, since neither of the Al superhydrophobic surfaces exhibit SLAFs less than ∼10%, we prepared superhydrophobic Ti alloy surfaces according to previously published literature.[12,13] Here, the Ti alloy underwent one-pot anodization in an aqueous electrolyte of $NaOH/H_2O_2$, yielding a sponge-like morphology with hierarchical micro/nanostructures (Figure 1d_1). Morphological parameters, calculated from laser scanning microscopy images, demonstrate a Wenzel roughness parameter of ∼2.5 and an arithmetic mean value of 0.7 ± 0.1 μm (Figure 1d_2). The latter value is substantially lower than that of the Al samples. The as-anodized Ti alloy samples (A-Ti) were subsequently FS-treated to reduce the surface energy. EDS analysis revealed the presence of Ti, Al, and V from the Ti6Al4V alloy, as well as increased oxygen content resulting from electrochemical anodization (Figure S3b and Table S1). Additionally, the analysis shows higher concentrations of fluorine and phosphorus from the FS coating, attributed to the increased surface roughness. The EDS analysis also reveals a uniform coverage of the FS on the A-Ti/FS samples (Figure 1d_3). XPS measurements confirm the EDS results, demonstrating FS surface coverage on the A-Ti/FS substrate comparable to that on Al (Figure S6 and Table S3).

The goniometric measurements of the A-Ti/FS samples show CA values of 171.5° ± 8.5°, with CA values during both infusion and withdrawal of the drop volume comparable to those of the Al samples (Figure 2c_{1-2}). The as-anodized Ti alloy samples exhibit a brown color in air (Figure 2c_3). However, when immersed in water, these samples show mirror-like reflectance. The plastron in the A-Ti/FS samples is continuous with a few randomly distributed pinning points, with a solid−liquid area fraction of less than 1% (Figure 2c_{4-5}). Thus, as all samples demonstrate comparable goniometric parameters, identifying the most promising superhydrophobic surfaces is difficult. Concurrently, direct imaging of plastron using optical microscopy is feasible, primarily on continuous plastron. However, this method may interfere with the substrate's optical properties, as evidenced by the E-Al/FS case, complicating direct plastron analysis.

To overcome the complexity of analyzing plastron by optical reflectance microscopy, we employed the drop adhesion force (DAF) method to indirectly measure plastron characteristics. This simple and effective method detects the presence of plastron and evaluates its stability and uniformity. It also calculates the advancing and receding CAs, enabling a rapid assessment of the Cassie−Baxter surfaces. Furthermore, the DAF method can evaluate the extent to which plastron can retain its structural integrity under diverse external forces and in different environments. We recently demonstrated a linear relationship between drop adhesion force and the solid−liquid area fraction.[27] The latter enables the identification of the most promising superhydrophobic surface candidates for their plastron characteristic evaluation in minutes.

Basic Drop Adhesion Force Setup for Plastron Assessment

Figure 3a summarizes the basic experimental setup used to correlate the plastron developed on the E-Al/FS, EA-Al/FS, and A-Ti/FS substrates with DAF. The B−Al/FS samples, which have Wenzel wetting, were used as a control. The basic DAF setup consists of several steps. First, the drop of a known volume is brought into contact with the surface and left to rest for 0.25 s. Then, the drop is pressurized at a constant rate until

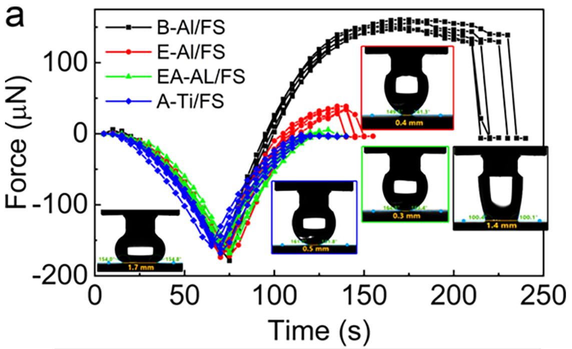

b

Sample	CA at force maximum (deg.)	CA at maximum pressing distance (deg.)	Drop contact line at force maximum (mm)
B-Al/FS	97.0	146.7	1.4
E-Al/FS	145.2	157.0	0.4
EA-Al/FS	164.3	158.2	0.3
A-Ti/FS	161.4	154.4	0.5

Figure 3. (a) Drop adhesion force was measured on the B−Al/FS, E-Al/FS, EA-Al/FS, and A-Ti/FS substrates by using DI water. The pressing distance was set to 0.4 mm. The inset images are digital images of the drop at the maximum compression distance (bottom left image) and maximum force distance (right images). The rim color of the inset images corresponds to the measured data. (b) CA values were measured at the maximum force and maximum pressing distance along with the drop contact line. Note that B−Al/FS is the Wenzel (control) surface, while others are Cassie−Baxter surfaces.

it reaches a predefined distance. The process ends with pulling off the drop at a constant rate until full recovery or tear-off.

Figure 3b summarizes the calculated CA values at the maximum pressing distance and maximum force, i.e., the point of maximal drop elongation, along with the drop contact line length at the maximum force. As shown, the B−Al/FS samples exhibit elevated DAF values of 152.8 ± 5.8 μN, attributed to the Wenzel-type wetting, i.e., conformal wetting without plastron. The E-Al/FS and EA-Al/FS samples exhibited noticeably lower DAF values of 34.3 ± 3.8 and 2.8 ± 1.9 μN, respectively. Meanwhile, the A-Ti/FS samples yielded negative values of −2.4 ± 0.8 μN, indicating that water drops do not adhere to these surfaces (Figure 3a). It should be noted that negative values of the maximum drop adhesion force are not physically meaningful. They can be attributed to the loss of test liquid due to evaporation over the course of the experiment. The discrepancy between the missing drop weight and the nearly zero pulling-off force results in an apparent negative force. Comparative analysis of the SHS samples revealed comparable dropline length at maximum force, ranging from 0.3 to 0.5 mm (Figure 3b). The results of the DAF analysis confirm the previously measured plastron by optical reflectance microscopy, thereby suggesting that an increase in the SLAF values is associated with a corresponding rise in DAF.[27]

The basic DAF setup already reveals substantial differences between the Wenzel and Cassie−Baxter surfaces, i.e., the existence of plastron and its SLAF coverage. For superhydrophobic surfaces to be applicable across a range of applications, however, they must exhibit resistance to specific environmental conditions while maintaining their performance over the designated lifetime of the application. In other words, plastron on Cassie−Baxter surfaces should be thermodynamically stable to sustain significant perturbations in the surrounding environmental conditions.[12] Previously, optical reflectance microscopy was used to measure plastron for stability frameworks.[13] Yet, the overall measurements, which encompass the roughness of highly rough/porous surfaces and the solid−liquid area fraction, continue to present challenges. Young's CA, estimated by the most stable CA, is barely accessible. It is subsequently replaced by advancing and receding CAs. In most cases, however, these measurements do not allow for an unambiguous determination of plastron stability.[12] The aforementioned challenges resulted in lengthy measurements, while goniometric measurements are simply insensitive and do not yield the required information. Thus, we extend the basic DAF setup to determine the sustainability of plastron characteristics under diverse environmental conditions.

Drop Adhesion Force Setup for Assessment of Long-Term Stability of Plastron

Figure 4 demonstrates the plastron for long-term stability experiments. In these experiments, the water drop was maintained at its maximum pressing distance of 0.6 mm for 5 min before being pulled off. During that delay, the drop underwent partial evaporation, indicating a decrease in its mass/force. As expected, the DAF values of the B−Al/FS samples increased considerably after a 5 min delay, reaching 212.2 ± 4.6 μN (a 39% increase compared to the basic setup value), despite substantial water drop evaporation during the experiment. The increase in DAF can be attributed to the larger contact drop footprint on the surface, because a greater compression distance was applied to offset water drop evaporation.

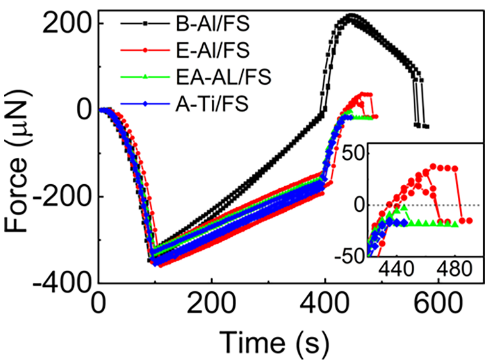

Figure 4. Drop adhesion force was measured on the B−Al/FS, E-Al/FS, EA-Al/FS, and A-Ti/FS substrates with deionized (DI) water. The drop was held in place for an additional 5 min at a maximum pressing distance. The pressing distance was set to 0.6 mm to compensate for the drop's partial evaporation. Note that the B−Al/FS is the Wenzel (control) surface, while the others are Cassie−Baxter surfaces.

The DAF values of the E-Al/FS and EA-Al/FS samples increased by 34 and 335%, reaching 45.9 ± 6.0 and 9.4 ± 1.9 μN, respectively. This substantial increase in DAF is due to the relative decrease in SLAF of the E-Al/FS samples, which is considerably smaller than that in the EA-Al/FS samples. Both increases in drop adhesion forces occur due to (*i*) the enlarged contact footprint of the drop on the surface, and more importantly, (*ii*) the metastability of plastron on those surfaces.

Meanwhile, the A-Ti/FS samples displayed no alteration in their DAF values, maintaining a negative value of −2.4 ± 1.7 μN. This is attributed to plastron stability, as evidenced by optical reflectance microscopy, particularly in the case of continuous plastron, as observed in the EA-Al/FS and A-Ti/FS samples. Snapshots of plastron that developed on the EA-Al/FS and A-Ti/FS surfaces were captured by the optical reflectance microscopy imaging at 1 min intervals for a total duration of 5 min (see Movies S1 and S2). As shown in Movie S1, the EA-Al/FS plastron experiences temporal dissolution, thereby exposing new pinning points wetted by water. Concurrently, the A-Ti/FS samples exhibited stability without plastron degradation (Movie S2). Thus, this simple and rapid experiment already demonstrates substantial differences in plastron performance between the EA-Al/FS and A-Ti/FS samples, despite both possessing continuous plastron.

Drop Adhesion Force Setup for the Pressure Stability Assessment of Plastron

Plastron pressure stability was examined by increasing the compressing distance from 0.2 to 0.4 mm while keeping the drop volume constant. This resulted in applied pressures of 21 and 30 Pa, respectively (Figure 5a−c). These experiments were conducted for durations ranging from 1.8 to 2.5 min for pressure distances of 0.2 and 0.4 mm, respectively. As shown, the increase in pressure distance led to a 40% increase in DAF values of the E-Al/FS samples, ranging from 44.9 ± 7.5 to 62.7 ± 17.1 μN (Figure 5a). The DAF values of the EA-Al/FS and A-Ti/FS samples did not substantially change, ranging from 2.7 ± 1.3 to 2.9 ± 3.3 μN for EA-Al/FS and −0.5 ± 0.6 to −2.5 ± 2.0 μN for A-Ti/FS. The latter indicates that, under applied conditions, plastron remains stable despite the drop's enlarged contact footprint on the surface (Figures 5b,c and S9).

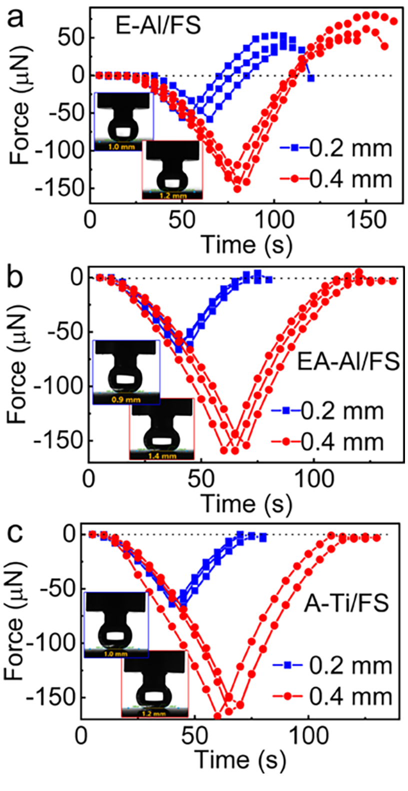

Figure 5. Drop adhesion force was measured on the E-Al/FS (a), EA-Al/FS (b), and A-Ti/FS (c) superhydrophobic samples as a function of increased compressing distance from 0.2 to 0.4 mm. The inset images were taken at a maximum compression distance.

Drop Adhesion Force Setup for Assessing Plastron Stability in Seawater

Due to the negligible presence of charge carriers (e.g., ions) and other impurities (e.g., organic molecules), deionized (DI) water serves as a benchmark liquid used in goniometric measurements to evaluate wetting characteristics of a surface, providing consistent surface tension. However, the situation is considerably different in real aquatic environments. Fresh and seawater contain dissolved salts, ions, and organic matter that affect surface tension.[45,46] These constituents result in more diverse chemical and biological interactions with surfaces than DI water does. The latter influences the wetting performance. Thus, it is important to characterize superhydrophobic surfaces using real aquatic media.[43] Here, we used filtered natural seawater as an aquatic medium to evaluate the plastron on the developed superhydrophobic surfaces, and the results are summarized in Figures 6a−c and S10. Surface tension of seawater was measured using the Wilhelmy plate method and found to be 68.9 ± 0.1 mN m^{-1}. As shown, the E-Al/FS samples exhibit an approximately 50% increase in adhesion forces as compared to DI water, from 35.8 ± 2.6 to 53.8 ± 16.5 μN. This can be attributed to the high solid−liquid area fraction, which does not protect the Al surface from aggressive media, such as seawater, with a high halide ion content. Both substrates with continuous plastron demonstrate comparable adhesion forces in both DI and seawater during the experiments. However, the standard deviation was consid-

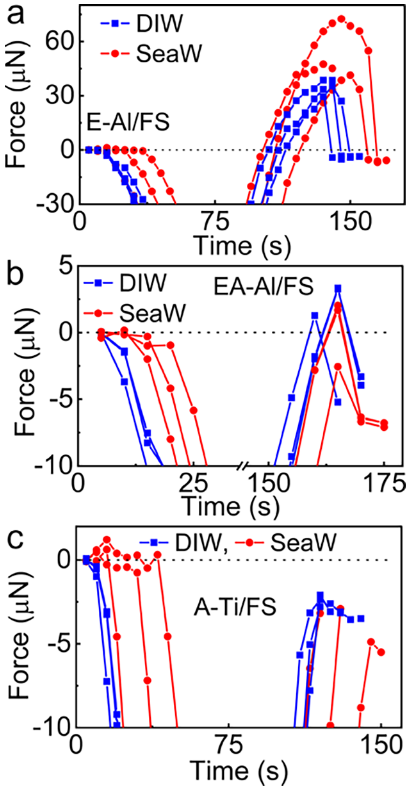

Figure 6. Comparison of the drop adhesion force on the E-Al/FS (a), EA-Al/FS (b), and A-Ti/FS (c) Cassie−Baxter samples between deionized water and seawater.

erably higher in seawater (Figure S10). In the absence of definitive evidence regarding the precise cause and considering the slight reduction in seawater surface tension, it is reasonable to hypothesize that the widespread presence of corrosive ions in seawater may already induce corrosion events on the Al surface.

These results highlight the significant impact of the chemical composition of aqueous media on the adhesive properties and the challenges posed by real aquatic environments due to halide ions and other constituents that disrupt the wetting performance. The consistent performance of continuous plastron substrates in both types of aquatic media suggests their robustness in diverse conditions, making them promising candidates for biomimetic antifouling and anticorrosion surface applications.

■ CONCLUSIONS

This research presents a simple and rapid method for analyzing the stability of air plastron developed on Cassie—Baxter surfaces through drop adhesion force measurements. Current characterization techniques for superhydrophobic surfaces primarily rely on goniometric wetting parameters such as contact angle (CA) and CA hysteresis. Though these parameters are easily obtainable, interpreting them poses significant challenges. This is significant because our studies show that superhydrophobic surfaces with comparable goniometric characteristics exhibit remarkably different wetting performances.[7,13] Such ambiguity in characterizing superhydrophobic surfaces limits their practical application substantially.

We recently proposed to measure plastron on Cassie—Baxter surfaces directly by optical reflectance microscopy.[12,13] The technique provides a high field of view (*e.g.*, millimeters) with a micrometer lateral resolution. However, as demonstrated in this study, the method faces challenges on surfaces with nonuniform coloration, where plastron can interfere with surface reflectance. To further simplify plastron measurements and make them independent of solid surface conditions, we propose using the drop adhesion force (DAF) method as an indirect measure.[27] This method enables the rapid evolution of Cassie—Baxter surfaces, which helps predict plastron coverage.

This study further advances plastron characteristics, quantifying their stability and longevity across various aquatic environments. Here, we demonstrate that, by simple modifications of the basic DAF setup, all of these particle parameters can be obtained within minutes and even before measuring more complex parameters such as surface roughness and various CAs. The proposed DAF setups will assist the wetting community in identifying the most promising candidates for wetting-repellent applications. Overall, this study circumvents the limitations frequently associated with measuring the wetting properties of superhydrophobic surfaces and plastron estimation. A key implication of this study is the necessity of evaluating surface interactions in realistic environments to better understand and optimize surfaces for their intended applications in the field of aquatic science and technology. This is crucial because superhydrophobic surfaces depend on a plastron for various applications, including corrosion and biofouling resistance, ice adhesion, and friction-free floating. However, for the DAF-SLAF method to be widely adopted, it must be standardized. This is due to the variety of tip geometries and experimental conditions.

■ ASSOCIATED CONTENT

Supporting Information

The Supporting Information is available free of charge at https://pubs.acs.org/doi/10.1021/acs.langmuir.5c06133.

(1) Calculations of CA using the Ellipse and Laplace—Young fits, (2) solid—liquid area fraction analysis, (3) energy-dispersive X-ray spectroscopy of the prepared SHS samples, (4) XPS measurements of the O 1s peak in B—Al/FS, E-Al/FS, and EA-Al/FS samples, (5) contact angle of the B—Al/FS sample, (6) high-resolution XPS F 1s and P 2p peaks of the E-Al/FS, EA-Al/FS, and A-Ti/FS samples, (7) optical reflectance microscopy images of the E-Al/FS samples in air and underwater, (8) optical reflectance microscopy images of the EA-Al/FS samples in air and underwater, (9) statistical analysis of DAF experiments as a function of pressing distance, and (10) statistical analysis of DAF experiments as a function of aquatic media (PDF)

Optical reflectance microscopy imaging of plastron on EA-Al/FS samples immersed in water (MP4)

Optical reflectance microscopy imaging of plastron on the A-Ti/FS samples immersed in water (MP4)

■ AUTHOR INFORMATION

Corresponding Author

Alexander B. Tesler — *Department of Physics, Biophysics Group, Friedrich-Alexander-Universität Erlangen-Nürnberg, Erlangen 91052, Germany; Department of Materials Engineering, Faculty of Engineering, Bar Ilan University, Ramat-Gan 5290002, Israel;* orcid.org/0000-0003-3425-7667; Email: alexander.tesler@biu.ac.il

Authors

Iana Fomicheva — *Fraunhofer Institute for Ceramic Technologies and Systems IKTS, Forchheim 91301, Germany; Department of Physics, Biophysics Group, Friedrich-Alexander-Universität Erlangen-Nürnberg, Erlangen 91052, Germany; Institute for Nanotechnology and Correlative Microscopy gGmbH (INAM), Forchheim 91301, Germany*

Petr Druzhinin — *Fraunhofer Institute for Ceramic Technologies and Systems IKTS, Forchheim 91301, Germany; Institute for Nanotechnology and Correlative Microscopy gGmbH (INAM), Forchheim 91301, Germany*

Mariia Pavlovska — *KRÜSS GmbH, Hamburg 22453, Germany*

Karen Ferner — *KRÜSS GmbH, Hamburg 22453, Germany*

Daniel Frese — *KRÜSS GmbH, Hamburg 22453, Germany*

George Sarau — *Fraunhofer Institute for Ceramic Technologies and Systems IKTS, Forchheim 91301, Germany; Institute for Nanotechnology and Correlative Microscopy gGmbH (INAM), Forchheim 91301, Germany; Max Planck Institute for the Science of Light, Erlangen 91058, Germany*

Anca Mazare — *Department of Materials Science, Institute for Surface Science and Corrosion, Friedrich-Alexander-Universität Erlangen-Nürnberg, Erlangen 91058, Germany;* orcid.org/0000-0002-4836-946X

Wolfgang H. Goldmann — *Department of Physics, Biophysics Group, Friedrich-Alexander-Universität Erlangen-Nürnberg, Erlangen 91052, Germany;* orcid.org/0000-0003-0738-2665

Ben Fabry − *Department of Physics, Biophysics Group, Friedrich-Alexander-Universität Erlangen-Nürnberg, Erlangen 91052, Germany*

Silke H. Christiansen − *Fraunhofer Institute for Ceramic Technologies and Systems IKTS, Forchheim 91301, Germany; Institute for Nanotechnology and Correlative Microscopy gGmbH (INAM), Forchheim 91301, Germany; Physics Department, Freie Universität Berlin, Berlin 14195, Germany;* orcid.org/0000-0002-4908-4087

Complete contact information is available at: https://pubs.acs.org/10.1021/acs.langmuir.5c06133

Author Contributions

All authors contributed to the writing of the manuscript. All authors approved the final version of the manuscript. I.F. and P.D contributed equally.

Notes

The authors declare no competing financial interest.

■ ACKNOWLEDGMENTS

I.F., W.H.G., B.F., and A.B.T. thank the Deutsche Forschungsgemeinschaft (DFG) (award number 540989797) for financial support. I.F., G.S., and S.C. were supported by the European Union's H2020 research and innovation program through the Marie Sklodowska-Curie grant agreement AIMed ID: 861138, and the research projects 4D+ nanoSCOPE ID: 810316 and LRI ID: C10, STOP ID: 101057961; the German Research Foundation (DFG) within the research project UNPLOK ID: 523847126, and from the "Freistaat Bayern" and the European Union within the project Analytiktechnikum für Gesundheits- und Umweltforschung AGEUM, project (StMWi-43-6623-22/1/3).

■ REFERENCES

(1) Parvate, S.; Dixit, P.; Chattopadhyay, S. Superhydrophobic Surfaces: Insights from Theory and Experiment. *J. Phys. Chem. B* **2020**, *124* (8), 1323−1360.

(2) Li, L.; Wei, J.; Zhang, J.; Li, B.; Yang, Y.; Zhang, J. Challenges and strategies for commercialization and widespread practical applications of superhydrophobic surfaces. *Sci. Adv.* **2023**, *9* (42), eadj1554.

(3) Butt, H.-J.; Liu, J.; Koynov, K.; Straub, B.; Hinduja, C.; Roismann, I.; Berger, R.; Li, X.; Vollmer, D.; Steffen, W.; Kappl, M. Contact angle hysteresis. *Curr. Opin. Colloid Interface Sci.* **2022**, *59*, No. 101574.

(4) Quéré, D. Wetting and Roughness. *Annu. Rev. Mater. Res.* **2008**, *38*, 71−99.

(5) Vuckovac, M.; Latikka, M.; Liu, K.; Huhtamäki, T.; Ras, R. H. A. Uncertainties in contact angle goniometry. *Soft Matter* **2019**, *15* (35), 7089−7096.

(6) Liu, K.; Vuckovac, M.; Latikka, M.; Huhtamäki, T.; Ras, R. H. A. Improving surface-wetting characterization. *Science* **2019**, *363*, 1147−1148.

(7) Prado, L. H.; Hayek, S.; Mazare, A.; Erceg, I.; Sarau, G.; Christiansen, S.; Kamaleev, M.; Wurmshuber, M.; Lohbauer, U.; Goldmann, W. H.; Virtanen, S.; Tesler, A. B. Aerophilic Surfaces for Sustained Corrosion Protection of Metals Underwater. *Adv. Funct. Mater.* **2024**, *34* (44), 2407444.

(8) Poetes, R.; Holtzmann, K.; Franze, K.; Steiner, U. Metastable Underwater Superhydrophobicity. *Phys. Rev. Lett.* **2010**, *105* (16), No. 166104.

(9) Röhrig, M.; Mail, M.; Schneider, M.; Louvin, H.; Hopf, A.; Schimmel, T.; Worgull, M.; Hölscher, H. Nanofur for Biomimetic Applications. *Adv. Mater. Interfaces* **2014**, *1* (4), 1300083.

(10) Mehanna, Y. A.; Sadler, E.; Upton, R. L.; Kempchinsky, A. G.; Lu, Y.; Crick, C. R. The challenges, achievements and applications of submersible superhydrophobic materials. *Chem. Soc. Rev.* **2021**, *50* (11), 6569−6612.

(11) Martínez-Gómez, A.; López, S.; García, T.; de Francisco, R.; Tiemblo, P.; García, N. Long-Term Underwater Hydrophobicity: Exploring Topographic and Chemical Requirements. *ACS Omega* **2017**, *2* (12), 8928−8939.

(12) Tesler, A. B.; Kolle, S.; Prado, L. H.; Thievessen, I.; Böhringer, D.; Backholm, M.; Karunakaran, B.; Nurmi, H. A.; Latikka, M.; Fischer, L.; Stafslien, S.; Cenev, Z. M.; Timonen, J. V. I.; Bruns, M.; Mazare, A.; Lohbauer, U.; Virtanen, S.; Fabry, B.; Schmuki, P.; Ras, R. H. A.; Aizenberg, J.; Goldmann, W. H. Long-Lasting Aerophilic Metallic Surfaces Underwater. *Nat. Mater.* **2023**, *22* (12), 1548−1555.

(13) Tesler, A. B.; Nurmi, H. A.; Kolle, S.; Prado, L. H.; Karunakaran, B.; Mazare, A.; Erceg, I.; de Brito Soares, Í.; Sarau, G.; Christiansen, S.; Stafslien, S.; Alvarenga, J.; Aizenberg, J.; Fabry, B.; Ras, R. H. A.; Goldmann, W. H. Predicting plastron thermodynamic stability for underwater superhydrophobicity. *Commun. Mater.* **2024**, *5* (1), 112.

(14) Butt, H.-J.; Roisman, I. V.; Brinkmann, M.; Papadopoulos, P.; Vollmer, D.; Semprebon, C. Characterization of super liquid-repellent surfaces. *Curr. Opin. Colloid Interface Sci.* **2014**, *19* (4), 343−354.

(15) Nagy, N. Contact Angle Determination on Hydrophilic and Superhydrophilic Surfaces by Using r−θ-Type Capillary Bridges. *Langmuir* **2019**, *35* (15), 5202−5212.

(16) Nagy, N. Capillary Bridges on Hydrophobic Surfaces: Analytical Contact Angle Determination. *Langmuir* **2022**, *38* (19), 6201−6208.

(17) Reyssat, M.; Quéré, D. Contact Angle Hysteresis Generated by Strong Dilute Defects. *J. Phys. Chem. B* **2009**, *113* (12), 3906−3909.

(18) Qiao, S.; Li, S.; Li, Q.; Li, B.; Liu, K.; Feng, X.-Q. Friction of Droplets Sliding on Microstructured Superhydrophobic Surfaces. *Langmuir* **2017**, *33* (47), 13480−13489.

(19) Drelich, J. W. Contact angles: From past mistakes to new developments through liquid-solid adhesion measurements. *Adv. Colloid Interface Sci.* **2019**, *267*, 1−14.

(20) Zhang, S.; Zhao, L.; Yu, M.; Guo, J.; Liu, C.; Zhu, C.; Zhao, M.; Huang, Y.; Zheng, Y. Measurement Methods for Droplet Adhesion Characteristics and Micrometer-Scale Quantification of Contact Angle on Superhydrophobic Surfaces: Challenges and Opportunities. *Langmuir* **2024**, *40* (19), 9873−9891.

(21) Backholm, M.; Molpeceres, D.; Vuckovac, M.; Nurmi, H.; Hokkanen, M. J.; Jokinen, V.; Timonen, J. V. I.; Ras, R. H. A. Water droplet friction and rolling dynamics on superhydrophobic surfaces. *Commun. Mater.* **2020**, *1* (1), 64.

(22) Tan, Y.; Yang, J.; Li, Y.; Li, X.; Wu, Q.; Fan, Y.; Yu, F.; Cui, J.; Chen, L.; Wang, D.; Deng, X. Liquid-Pressure-Guided Superhydrophobic Surfaces with Adaptive Adhesion and Stability. *Adv. Mater.* **2022**, *34* (30), 2202167.

(23) Timonen, J. V. I.; Latikka, M.; Ikkala, O.; Ras, R. H. A. Free-decay and resonant methods for investigating the fundamental limit of superhydrophobicity. *Nat. Commun.* **2013**, *4* (1), 2398.

(24) Zhang, Y.; Wang, T.; Lv, Y. Durable Biomimetic Two-Tier Structured Superhydrophobic Surface with Ultralow Adhesion and Effective Antipollution Property. *Langmuir* **2023**, *39* (7), 2548−2557.

(25) Nagy, N. Determination of solid-liquid adhesion work on flat surfaces in a direct and absolute manner. *Sci. Rep.* **2024**, *14* (1), 29991.

(26) Lepikko, S.; Turkki, V.; Koskinen, T.; Raju, R.; Jokinen, V.; Kiseleva, M. S.; Rantataro, S.; Timonen, J. V. I.; Backholm, M.; Tittonen, I.; Ras, R. H. A. Droplet Friction on Superhydrophobic Surfaces Scales With Liquid-Solid Contact Fraction. *Small* **2025**, *21* (7), 2405335.

(27) Druzhinin, P.; Fomicheva, I.; Sarau, G.; Mazare, A.; Song, B.; Goldmann, W. H.; Christiansen, S.; Tesler, A. B. Drop Adhesion Force as a Measure of the Solid−Liquid Area Fraction on Cassie−Baxter Superhydrophobic Surfaces. *Langmuir* **2026**.

(28) Inoue, T.; Koyama, A.; Kowalski, D.; Zhu, C.; Aoki, Y.; Habazaki, H. Fluorine-Free Slippery Liquid-Infused Porous Surfaces Prepared Using Hierarchically Porous Aluminum. *Phys. Status Solidi (a)* **2020**, *217* (13), 1900836.

(29) Mazare, A.; Ulubas, M. H.; Kim, H.; Fomicheva, I.; Sarau, G.; Christiansen, S. H.; Goldmann, W. H.; Tesler, A. B. Binding Kinetics of Self-Assembled Monolayers of Fluorinated Phosphate Ester on Metal Oxides for Underwater Aerophilicity. *Langmuir* **2025**, *41* (3), 1868−1875.

(30) Tesler, A. B.; Sannomiya, T.; Vaskevich, A.; Sabatani, E.; Rubinstein, I. Highly Sensitive Colorimetric Detection of Early Stage Aluminum Corrosion in Water Using Plasmonic Gold Nanoparticle Films. *Adv. Opt. Mater.* **2018**, *6* (21), 1800599.

(31) Greczynski, G.; Hultman, L. Undressing the myth of apparent constant binding energy of the C 1 s peak from adventitious carbon in x-ray photoelectron spectroscopy. *Sci. Talks* **2022**, *1*, No. 100007.

(32) Drelich, J. Guidelines to measurements of reproducible contact angles using a sessile-drop technique. *Surface Innovations* **2013**, *1* (4), 248−254.

(33) Arthur, D.; Vassilvitskii, S. k-means++: the advantages of careful seeding. In *Proceedings of the eighteenth annual ACM-SIAM symposium on Discrete algorithms, New Orleans, Louisiana*; Society for Industrial and Applied Mathematics: Philadelphia, PA, 2007.

(34) Lloyd, S. Least squares quantization in PCM. *IEEE Trans. Inf. Theory* **1982**, *28* (2), 129−137.

(35) Seber, G. A. F. *Cluster Analysis*; John Wiley & Sons, Inc., 1984. .

(36) Späth, H. *Cluster Dissection and Analysis: Theory, FORTRAN Programs, Examples*; Ellis Horwood, 1985.

(37) Hom-on, C.; Triroj, N.; Horprathum, M.; Lertvanithphol, T.; Chananonnawathorn, C.; Limwichean, S.; Nuntawong, N.; Songsiriritthigul, P.; Nakajima, H.; Klamchuen, A.; Jaroenapibal, P. Hydrolysis corrosion of alumina thin films produced by pulse DC reactive magnetron sputtering at various operating pressures. *Ceram. Int.* **2021**, *47*, 9691−9700.

(38) Zähr, J.; Oswald, S.; Türpe, M.; Ullrich, H. J.; Füssel, U. Characterisation of oxide and hydroxide layers on technical aluminum materials using XPS. *Vacuum* **2012**, *86* (9), 1216−1219.

(39) Botelho do Rego, A. M.; Ferraria, A. M.; El Beghdadi, J.; Debontridder, F.; Brogueira, P.; Naaman, R.; Rei Vilar, M. Adsorption of Phenylphosphonic Acid on GaAs (100) Surfaces. *Langmuir* **2005**, *21* (19), 8765−8773.

(40) Sanz, O.; Echave, F. J.; Odriozola, J. A.; Montes, M. Aluminum Anodization in Oxalic Acid: Controlling the Texture of Al_2O_3/Al Monoliths for Catalytic Aplications. *Ind. Eng. Chem. Res.* **2011**, *50* (4), 2117−2125.

(41) Marmur, A. Underwater Superhydrophobicity: Theoretical Feasibility. *Langmuir* **2006**, *22* (4), 1400−1402.

(42) Lafuma, A.; Quéré, D. Superhydrophobic states. *Nat. Mater.* **2003**, *2* (7), 457−460.

(43) Awashra, M.; Mirmohammadi, S. M.; Meng, L.; Franssila, S.; Jokinen, V. Stable Air Plastron Prolongs Biofluid Repellency of Submerged Superhydrophobic Surfaces. *Langmuir* **2025**, *41* (3), 1807−1820.

(44) McCafferty, E. Sequence of steps in the pitting of aluminum by chloride ions. *Corros. Sci.* **2003**, *45* (7), 1421−1438.

(45) Aveyard, R.; Saleem, S. M. Interfacial tensions at alkane-aqueous electrolyte interfaces. *J. Chem. Soc., Faraday Trans. 1* **1976**, *72* (0), 1609−1617.

(46) Turner, D. R.; Croot, P. L.; Dickson, A. G.; Gledhill, M. Physicochemical controls on seawater. In *Treatise on Geochemistry*, 3rd ed., Anbar, A.; Weis, D. Eds.; Elsevier, 2025; pp 1−51.